Available online at www.sciencedirect.com

jmr&t Journal of Materials Research and Technology

journal homepage: www.elsevier.com/locate/jmrt

Original Article

Quantitative percussion diagnostics for evaluating porosity and surface roughness of cold sprayed and laser deposited materials

Mahsa Amiri [a,b], *Grant A. Crawford* [b], *James C. Earthman* [c,*]

[a] *Materials and Manufacturing Technology, University of California, Irvine, CA 92697-2585, USA*

[b] *Department of Materials and Metallurgical Engineering, South Dakota School of Mines and Technology, Rapid City, SD 57701, USA*

[c] *Department of Materials Science and Engineering, University of California, Irvine, CA 92697-2585, USA*

ARTICLE INFO

Article history:
Received 3 February 2021
Accepted 15 June 2021
Available online 21 June 2021

Keywords:
Quantitative percussion diagnostics
Cold spray
Non-destructive evaluation
Laser powder directed energy deposition
Additive manufacturing
Porosity

ABSTRACT

Quantitative percussion diagnostics (QPD) is a non-destructive evaluation method that has been used successfully in a number of applications. This technique involves a rod that is actuated to impact a specimen with a given amount of kinetic energy and the resulting mechanical response of the specimen as a function of time is measured using a piezoelectric force sensor. The mechanical energy returned to the rod is then analyzed. Because contact with the specimen is on the order of a few hundred microseconds, QPD can be used in situations and for specimen conditions (e.g. high temperature) that are not feasible for other nondestructive testing methods. The objective of the present study was to evaluate the use of QPD for characterization of defects in specimens fabricated using two additive manufacturing methods, i.e. cold spray deposition and laser powder directed energy deposition (LPDED). Cold spray specimens were produced using commercially pure nickel with varied process conditions including gas type (i.e. helium and nitrogen) and deposition rate. In addition, a Ti–6Al–4V specimen was manufactured using LPDED with varying porosity content. All specimens were characterized using both QPD and destructive methods (i.e. cross-sectional metallography) to compare results for observed defect characteristics. Cold spray specimens exhibited a lower energy return when they contained more porosity and/or surface roughness. Microscopic plastic deformation at highly porous surfaces was indicated during percussion testing that reached a saturation level after repeated percussion. Overall, the results showed that QPD can effectively evaluate cold spray and LPDED specimens for porosity and surface roughness.

* Corresponding author.
E-mail address: earthman@uci.edu (J.C. Earthman).

https://doi.org/10.1016/j.jmrt.2021.06.047

1. Introduction

Quantitative percussion diagnostics (QPD) is a recently developed nondestructive testing (NDT) method that has been performed using the Periometer® instrument (Perimetrics LLC, Los Angeles, CA). This testing modality has been used to detect and quantitatively analyze overall mobility as well as the presence of fine gap defects such as cracks associated with teeth [1] and dental implants [2,3]. The effectiveness of QPD has also been demonstrated to detect weak 'kiss' bonds in laminate composite structures [4,5]. The QPD testing system consists of a probe containing a force sensor that is actuated to tap a specimen. Upon the percussion of the probe against the specimen, force-time data are recorded by a piezoelectric sensor in the rod. This relatively low-level impact generates a maximum stress in the specimen that is nondestructive. The resulting force-time profile for each percussion, which is characteristic of the specimen, is recorded over the 0.2–0.4 ms that the rod is in contact with the specimen. Software in a computer interfaced to the percussion probe determines the mechanical energy returned to the rod based on the force measured versus time for 10 percussions each time a measurement is made [4–6]. Fig. 1 shows a schematic of the present QPD test system.

Normalized energy return (NER), i.e. the mechanical energy returned to the rod relative to the kinetic energy of the rod right before the impact, is plotted versus time as the QPD test result. Mechanical energy returned is defined as the force squared divided by the dynamic stiffness of the sensor in the percussion rod measuring this force. NER versus time can be used to determine loss coefficient, a damping parameter showing overall energy dissipation in a structure, and the normal fit error (NFE), a parameter that indicates the presence and severity of cracks and other fine–gap defects [1–4,6–9]. A lower amplitude for the NER can indicate more energy dissipation by the structure as a result of a severe defect or the presence of a higher number of a specific defects (e.g., porosity) in the structure. The volume of material tested depends on the attenuation of the percussion energy by damping processes [5,8]. Further details of the operation of output parameters of the QPD system are described elsewhere [1–4].

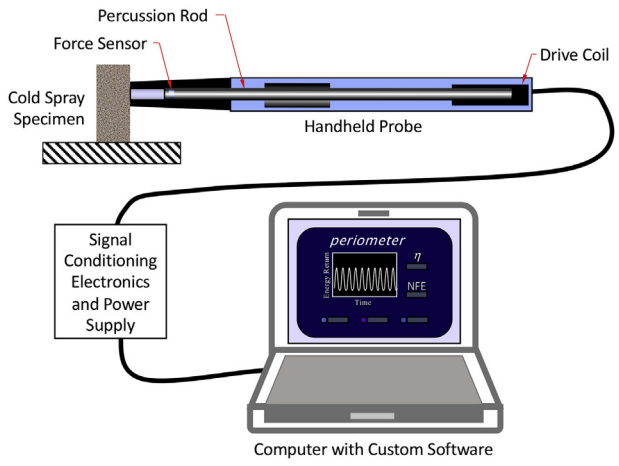

Fig. 1 – Schematic of the QPD test setup and hand piece that contains an instrumented percussion rod.

Conventional nondestructive testing (NDT) techniques used to detect defects in additively manufactured parts include ultrasonic inspection, thermography, X-radiography and shearography [10]. However, these techniques are typically not able to detect defects during the manufacturing process and can be either costly or difficult to use on large and complex shaped surfaces. By comparison, the attributes of QPD include (1) detection of any type of defect that dissipates mechanical energy applied to the material or constitutes a fine gap in the sample (e.g., a crack), (2) fast (about 5 s per measurement), portable, low-cost, and easy to operate making it practical to test large components in service, (3) can be used to characterize all types of materials and components, (4) the small diameter of the percussion rod tip (about 2 mm) makes it possible to test difficult to access areas, and (5) it provides quantitative data that indicate the structural integrity of the specimen. In addition, QPD can be used with specimens at high temperatures because the contact time between the percussion rod and the specimen is only on the order of a few hundred microseconds. These technical advantages directly address the need for an NDT device that can be used during both manufacturing and service to detect defects in localized areas within structures in various applications [4].

Cold gas dynamic spraying or cold spray (CS) is a solid-state deposition process, in which powder particles are accelerated to supersonic velocities (400–1200 m/s) in a gas stream at relatively low temperatures, below the melting point of the material. They impact the substrate and form a layer on its surface [11–13]. Powder particles typically experience severe plastic deformation during impact and bond to the substrate through a combination of mechanical interlocking and/or metallurgical bonding [11,12,14]. Because the deposition process occurs at temperatures well below the melting temperature of the feedstock material, the process limits oxidation, undesirable phase changes, and thermal stress development which often plague other thermal spray processes [12,13,15,16]. Over the past 10 years, cold spray technology has been used to produce wear and corrosion resistant coatings [16,17] and also to repair damaged aerospace and defense components [18]. More recently, cold spray technology has been developed for additive manufacturing (AM) [19,20].

Laser powder directed energy deposition (LPDED) is an established metal AM process that creates parts through layer-by-layer deposition. In this technique a laser beam is focused on the surface of the substrate and makes a pool of molten material, the powder feedstock is subsequently fed into the molten pool, melts and rapidly solidifies to create a layer of deposited material [21–25]. Compared to other common AM techniques (e.g., powder bed fusion) LPDED offers large build volumes and faster build rates, although at the expense of reduced feature resolution and surface quality. In addition, because powder is directly injected into the melt pool, LPDED offers the potential to functionally grade the properties of the build by changing the powder composition during the deposition process [23,24]. LPDED is commonly used to deposit a variety of metallic materials and metal matrix composites

including aluminum, nickel, stainless steel, and titanium alloys. Regarding the latter, Ti–6Al–4V components are commonly produced using LPDED for aerospace, defense, and medical applications, which take advantage of the excellent strength-to-weight ratio and corrosion resistance of the material [22–24,26].

Additive manufacturing techniques, despite their advantages, commonly exhibit defects that can originate from uncontrolled deposition conditions, unique part geometries, or poor-quality feedstock materials. Common defects include porosity, cracks, poor surface finish, and lack-of-fusion regions, which can lead to poor mechanical properties (e.g., reduced ductility, low strength, reduced fatigue life) [21,27]. Cold sprayed coatings, for example, can lack good interfacial adhesion between the substrate and coating often arising from poor bond line characteristics (lack of mechanical mixing and deforming), defects (e.g. pores or inclusions), or cracks along the interface. In addition, cold spray coatings can contain substantial porosity when particle deformation is insufficient, which results in reduced ductility and cohesive strength. In order to fully exploit the advantages of AM which enables custom production of unique part geometries in low volume, NDT methods are needed for accurate evaluation of defects to minimize the production of unacceptable parts and coatings without producing sacrificial test specimens. Furthermore, NDT methods are needed in materials repair processes since it is not possible to destructively test a repaired component. Our study evaluates QPD to understand the technique applicability for AM processes and understand how the unique characteristics of QPD may be exploited to offer an alternative or complementary method to other NDT methods. In addition, the sensitivity of QPD test to change in processing parameters (spray gas type and deposition rate in CS) and corresponding formed defects was studied.

2. Materials and methods

2.1. CS specimens

Commercially pure (CP) nickel powder (Amperit 176, H.C. Starck) was cold sprayed using a high pressure cold spray system (Gen III Max, VRC Metal Systems, Rapid City, SD). Table 1 summarizes the cold spray specimens evaluated in this study which were sprayed onto different substrates and under various processing conditions. Two specimens were sprayed on 304L stainless steel (SS) substrates using compressed air with a gas temperature and pressure of 600 °C and 5.5 MPa (800 psi), respectively. Nozzle standoff distance was 15 mm. By controlling the feedstock powder feed rate, two different specimens were produced, referred to as high (CS Ni–H, 210 μm/pass) and low (CS Ni-L, 90 μm/pass) deposition rates. Two other specimens of the same powder were sprayed on Inconel Alloy 600 substrates. The CS Ni–He specimen was sprayed using a helium carrier gas operating at 400 °C and 4.1 MPa (600 psi) and a standoff distance of 25 mm. The CS Ni–N_2 specimen was sprayed with a nitrogen carrier gas at 600 °C, 5.5 MPa (800 psi), and a 15 mm standoff distance. For all cold spray specimens, the substrate surface was grit blasted prior to deposition.

Table 1 – Specimen processing conditions and naming convention.

Specimen processing conditions	Specimen name
Cold sprayed CP-Ni in air, higher deposition rate	CS Ni–H
Cold sprayed CP-Ni in air, lower deposition rate	CS Ni-L
Cold sprayed CP-Ni in He	CS Ni–He
Cold sprayed CP-Ni in N_2	CS Ni–N_2
Laser deposited Ti–6Al–4V billet	LD Ti64

2.2. Laser deposited specimen

A billet (1.5 cm × 2.2 cm × 9.4 cm) of Ti–6Al–4V alloy was produced via laser powder directed energy deposition (LPDED) using a modified laser engineering net shaping (LENS) system (Optomec) with a 3 kW laser to examine the ability of QPD to detect internal porosity for this additive manufacturing process. Fig. 2 provides an image of the Ti–6Al–4V billet. Porosity content was varied as a function of billet height (i.e. greater porosity at the top) by increasing oxygen gas fed during the deposition. Ti–6Al–4V powder (Reading Alloys) with a particle size range of 44–105 μm was used. Laser power of 710 W and Ar carrier gas flow rate of 1.5 L/min were used for deposition. The complete build comprised 225 layers. It is common for LPDED specimens to show variations in the microstructure and properties as a function of build height. Among others, this can be often attributed to variations in heat dissipation and tempering. For instance, in many cases the porosity content near the substrate is elevated due to increased heat conduction and reduced melt pool temperatures. In this study, however, oxygen content within the process chamber was increased during the deposition process, in order to have higher porosity at the top of the billet. Table 1 summarizes the manufacturing process for specimens and their corresponding assigned names.

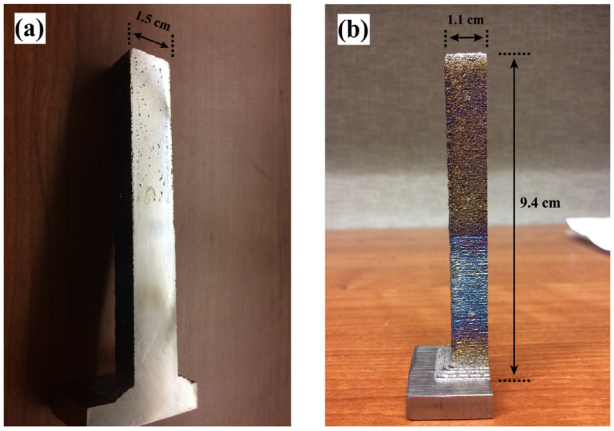

Fig. 2 – Shape of the LPDED Ti–6Al–4V specimen showing (a) polished and (b) as deposited surfaces. The images show the billet after being cross-sectionally polished.

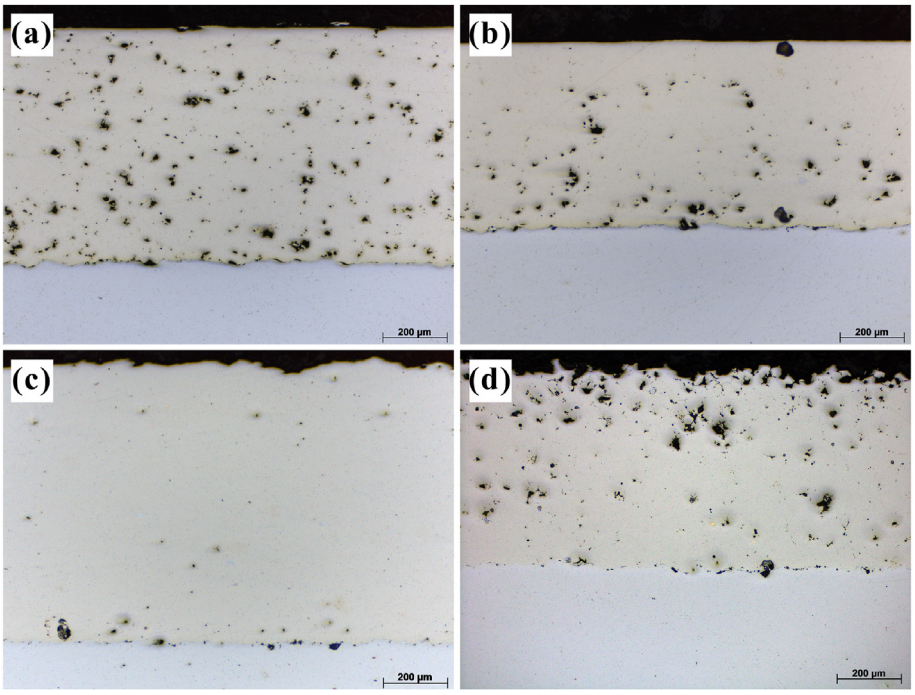

Fig. 3 – Optical micrographs of polished sections revealing porosity content: (a) CS Ni–H, (b) CS Ni-L, (c) CS Ni–He, and (d) CS Ni–N_2.

2.3. *Specimen characterization*

QPD was performed using the Periometer instrument (Perimetrics, LLC) on all of the specimens. The resulting normalized energy return-time plots were analyzed and normalized energy return at peak (peak NER) values were determined. Three consecutive QPD measurements (M1 to M3) were conducted at each specific location on the surface. Each test measurement is made from 10 percussions (P1 to P10) that are displayed by the software as energy return vs. time.

Three different locations on the coating surface of each CS specimen were tested. For LPDED Ti–6Al–4V specimen QPD was performed at the bottom and top regions of the billet to compare the effect of the internal porosity content on the QPD results. The billet was sectioned and polished from one side and was QPD tested on both the as deposited (rough) and the polished (smooth) surfaces, to also investigate the effect of surface roughness on the test results.

Adhesion strengths of CS specimens were measured according to ASTM D4541 [28] using a portable pull-off adhesion testing instrument (PosiTest ATA, DeFelsko, Ogdensburg, NY, USA). An Al pull-stub (10 mm in diameter) was bonded to the top surface of the coating using a high strength adhesive (glue) with a bond strength of 69 MPa. The device pulled the pull-stub until failure (either cohesive or adhesive) and the stress at failure was recorded. Three measurements were performed for each CS specimen and the average and standard deviation were determined.

Cross-sectional optical metallography was performed to measure porosity content and identify coating defects (e.g., cracks or bond line defects). CS CP-Ni specimens were cross-sectioned at the locations where QPD was implemented, and subsequently ground and polished with 9 µm, 3 µm, 1 µm and 0.05 µm diamond suspensions. Porosity content of the coatings was measured based on the optical microscopy images according to ASTM E2109-01 [29] standard for measuring porosity in thermal sprayed coatings. For each specimen, percent area porosity on 20 images was averaged with a magnification of 20 times for a resolution of 3.67 pixels/µm. Image J software was used for analyzing the images and measuring area percentage porosity. LD Ti64 specimen was ground and polished using standard procedures and subsequently imaged using a Leica Z16 APO optical macroscope.

A laser scanning confocal microscope (Keyence VK-X250) was utilized to investigate the surface profile of the impression caused by the QPD test on CS specimens. This was conducted to analyze the QPD surface impression and determine if QPD testing resulted in permanent deformation on the specimen surface.

3. Results and discussion

3.1. *CS CP-Ni coatings*

Fig. 3 shows microscopic images of polished cross-sections of the four CS CP-Ni specimens. Porosity of the CS CP-Ni coatings in area percentage was measured and is presented in Fig. 4. Higher porosity was observed for CS Ni–H, where the deposition rate (deposition thickness per pass) was greater and a thicker coating resulted (Fig. 3(a-b) and Fig. 4). It can also be clearly seen that porosity content is lower when He was used rather than N_2 (Fig. 3(c-d) and Fig. 4). In Fig. 3(d) there are two regions distinguishable in the coating sprayed with N_2: an

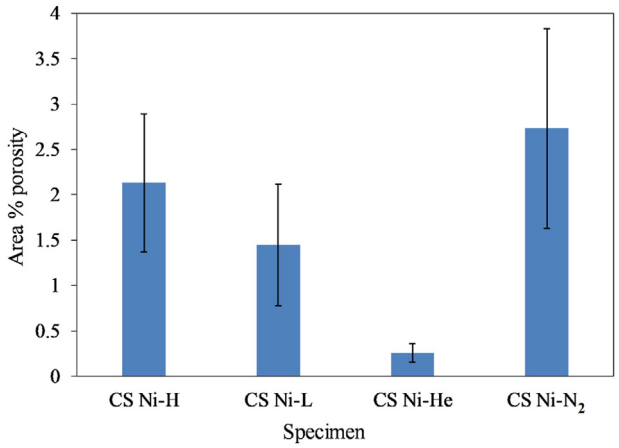

Fig. 4 – Area percentage porosity of CS Ni coatings. The positive and negative error bars each correspond to one standard deviation.

outer region with higher porosity and a denser inner region with lower porosity. This happens when some particles do not experience large enough plastic deformation or flattening during impact which leads to the generation of inter-splat porosities. These particles will be later tamped by successive impacts from the particles of the next layers. This is called tamping (or peening) effect which results in densification of porous regions throughout the deposition process [12].

Adhesion strength values for CS specimens are presented in Table 2. It was observed that the specimen sprayed with He has a higher adhesion strength than the one sprayed with N_2. In addition, comparing the compressed air depositions, the specimen sprayed with a lower deposition rate exhibited a greater adhesion strength compared to the high deposition rate. Finally, we note that the samples deposited in air (CS Ni–H and CS Ni-L) exhibited lower adhesion strength compared to that for the specimens sprayed in He and N_2. This difference is consistent with the findings of Li and coworkers [30] who showed that observed reductions in adhesion strength for CS Cu samples sprayed in air and He or N_2 could be attributed to presence of a thicker oxide film on the powder particles upon impact with the substrate.

NER-time plots for CS CP-Ni specimens for one of the test locations from each specimen are presented in Figs. 5 and 6. For clarity four (i.e., P1, P4, P7, and P10 where P1 represents the first and P10 represents the 10^{th} percussion) of the 10 percussions in each measurement are plotted in these figures. Fig. 5 compares the effect of the change in deposition rate, and Fig. 6 shows the plots for the two different spray gases. Little difference in the percussion responses can be observed in Fig. 5 for the different deposition rates with energy return being slightly lower for the first few percussions for CS Ni–H. However, clear differences can be seen when comparing the energy return vs. time plots for He and N_2 depositions shown in Fig. 6. Higher energy return was observed, and fewer percussions were required to reach the maximum energy return when He was used compared to that for CP-Ni sprayed in N_2.

The peak energy return can also increase as number of percussions at one location increases, particularly during the first measurement (M1). This is attributed to the strain hardening of splats and flattening of the rough or porous surface by localized plastic deformation. This effect will be more pronounced if the surface is rougher, since there will be higher stresses applied on each splat in contact with the probe. Also, when the surface material is softer, it should deform more and therefore strain harden more as a result of each percussion with a constant load. After successive percussions, this deformation should decrease. As a result, the increase in the energy return becomes smaller after multiple percussions so that no change in energy return is observed and a saturation in surface hardening is reached. Surface hardening due to percussion was pronounced for the coating sprayed with N_2 (Fig. 6(b)), whereas for the coating sprayed with He (Fig. 6(a)) the energy return is nearly unchanged with increasing percussions (P1 to P10) and from the first to third (M1 to M3) measurements.

Based on the present percussion data (Figs. 5 and 6), pronounced cracking or debonding did not exist in any of the specimens. Cracks, decohesions, debondings, and openings, usually result in a significant change in the shape of the energy return-time response. This change in shape can be manifest in the appearance of shoulders on the main peak, extra peaks, and/or a considerable drop in the value of the peak NER, which persists within increasing number of percussions [1,2,4]. In the present study, the peaks for all of the specimens were nearly symmetric and uniform in shape, which indicates that localized defects were likely not present. Metallographic investigation confirmed the absence of cracks and debondings as shown in Fig. 3.

Peak values of normalized energy return for CS CP-Ni specimens for all locations and for all the three test measurements are shown in Fig. 7. Arrows and error bars in this figure show the peak NER range, with the lowest value of the arrow/error bar showing the minimum and the highest value showing the maximum of the peak NER amongst 10 percussions in each measurement. Wherever there was a general sequential increase in the peak NER with increasing percussions an arrow was used, and wherever a variation in peak NER was independent of percussion number a normal error bar was used.

Porosity and peak NER values for the CS Ni specimens are listed together in Table 3 for comparison. The peak NER values are for the third measurement at a given location (M3) to minimize surface roughness effects. In addition, Student's T-test p-values are given for paired sets of porosity data in Table 4 and for paired sets of peak NER data in Table 5. A p-value below 0.05 is generally considered indicative of a significant statistical difference between the paired sets. It can be seen in Table 3 that Peak NER increases significantly when porosity

Table 2 – Adhesion strength values for cold sprayed specimens.

Specimen	Adhesion Strength (MPa)
CS Ni–H	13.8 ± 0.3
CS Ni-L	15.5 ± 1.0
CS Ni–He	glue failure
CS Ni–N_2	37.5 ± 4.8

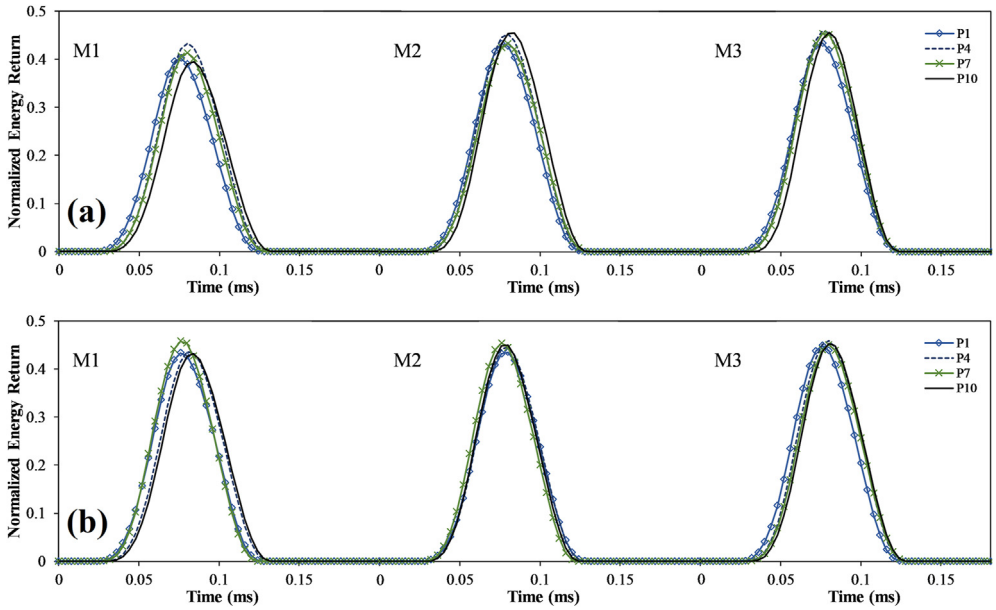

Fig. 5 – NER-time plots for CP-Ni specimens sprayed at different deposition rates. Plots in (a) correspond to the first, second and third test measurements at a specific location on the coating surface for CS Ni–H. Plots in (b) correspond to the first, second and third test measurements at a specific location on the coating surface for CS Ni-L. (M1, M2 and M3 represent three consecutive test measurements at one location on the coating surface, and P1, P4, P7, and P10 represent the first, fourth, seventh, and tenth percussion, respectively).

decreases significantly when comparing CS Ni–H to CS Ni-L and CS-Ni He to CS Ni–N_2. Some p-values that are greater than 0.05 in Tables 4 and 5 (shaded) indicate that some mean values cannot be considered significantly different (highlighted). This inability to differentiate the peak NER values for these paired sets is likely related to the difference in adhesion strengths between specimens sprayed at different deposition rates in air and the specimens sprayed with He and N_2. Specifically, it appears that other differences in the microstructures that affect adhesion strength such as oxidation can

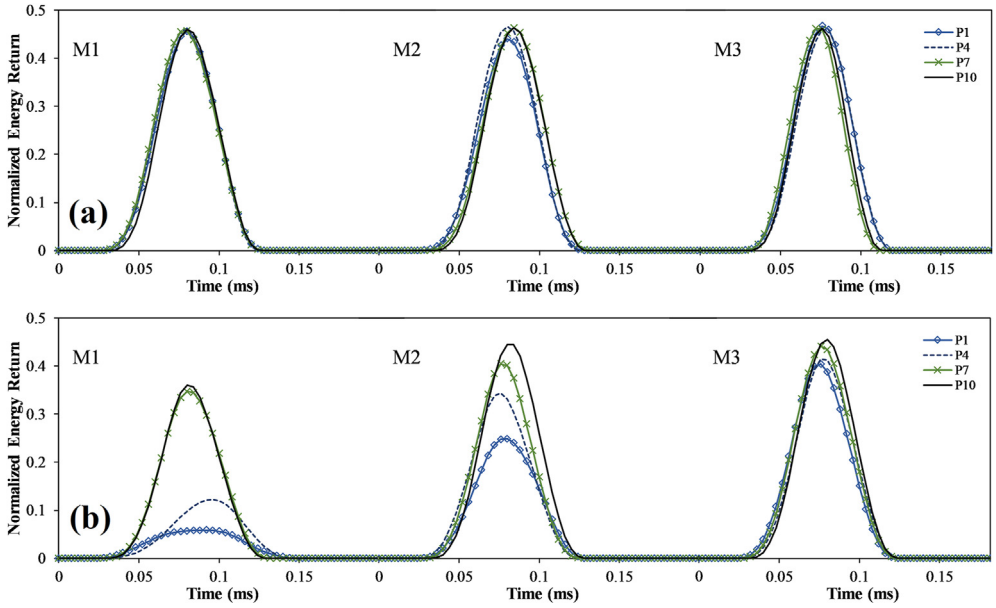

Fig. 6 – NER-time plots for CP-Ni specimens sprayed with He and N_2. Plots in (a) correspond to the first, second and third test measurements at a specific location on the coating surface for CS Ni–He. Plots in (b) correspond to the first, second and third test measurements at a specific location on the coating surface for CS Ni–N_2. (M1, M2 and M3 represent three consecutive test measurements at one location on the coating surface, and P1, P4, P7, and P10 represent the first, fourth, seventh, and tenth percussion, respectively).

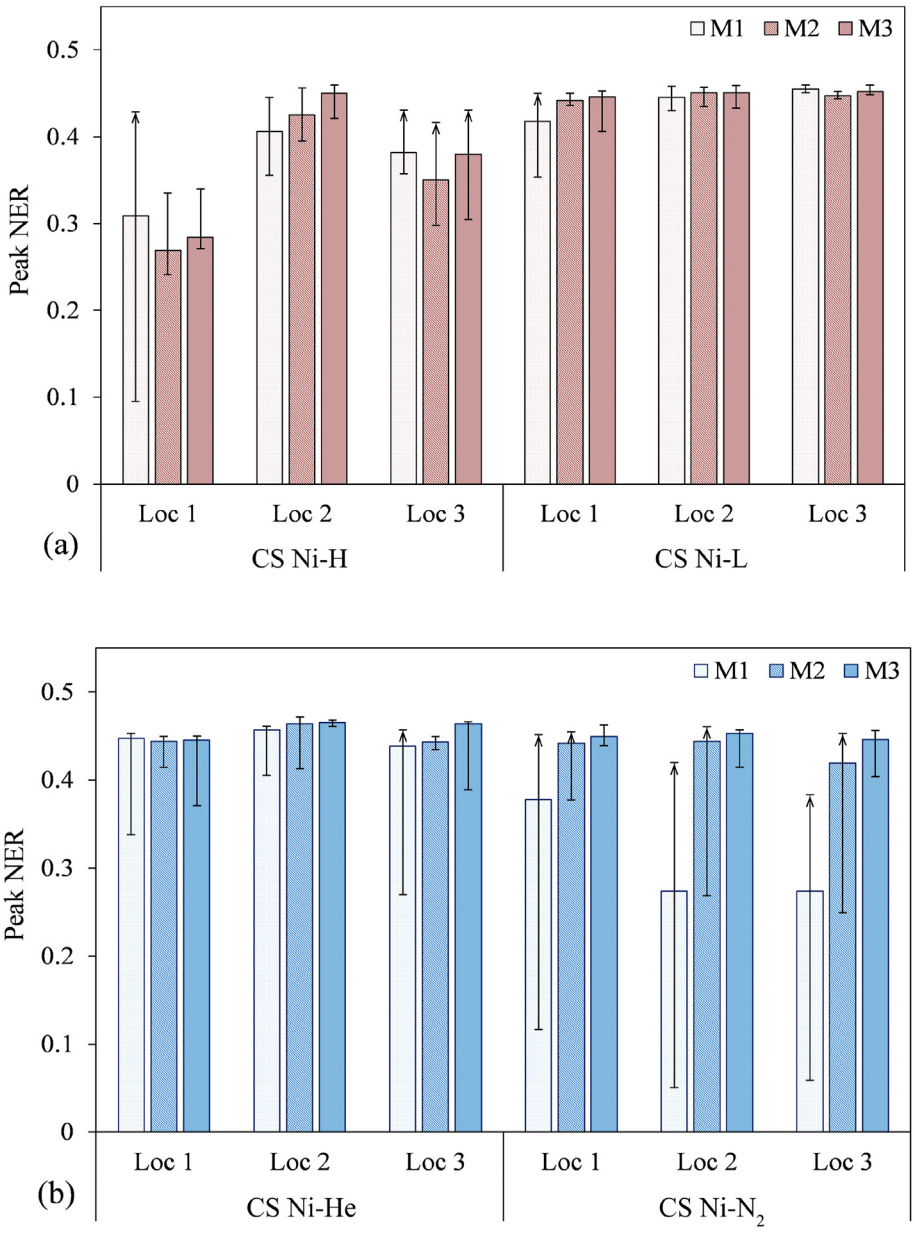

Fig. 7 – Peak NER values for CP-Ni specimens sprayed; a) at the two different deposition rates, b) with He and N_2. Each bar shows the median and the start (low value) and end (high value) of the arrows/error bars show the minimum and maximum of peak NER values amongst the 10 percussions.

compensate somewhat for the overall presence of porosity. For example, an increased presence of oxides in the specimens cold sprayed in air is possible given the other carrier gases (He and N_2) [30]. In addition, we note that the porosity along the substrate interface seemed to be lower for CS Ni–N_2 compared to that for either CS Ni-L or CS Ni–H, even though CS Ni–N_2 exhibited the highest overall porosity. This apparent difference in porosity distribution is consistent with the higher adhesion strength for CS Ni–N_2 compared to that for CS Ni-L and CS Ni–H. In sum, the present results suggest that while peak NER is affected by porosity it can also be affected by other microstructural characteristics that influence the damping capacity of the material.

Table 3 – Comparison of mean %Area Porosity and mean Peak NER values for the third QPD measurement.

Specimen	Area% porosity	Peak NER (M3)
CS Ni–H	2.13	0.374
CS Ni-L	1.45	0.448
CS Ni–He	0.26	0.452
CS Ni–N_2	2.73	0.444

Lower average peak NER was observed for CS Ni–H compared to CS Ni-L (Fig. 7(a)). This observation is consistent with the adhesion results in Table 2, which indicated lower adhesion strength for CS Ni–H than CS Ni-L. This specimen was sprayed with a greater deposition rate which

Table 4 – Paired Student's T-test p-values for %Area Porosity means for paired data sets.

Specimen	CS Ni–H	CS Ni-L	CS Ni–He	CS Ni–N_2
CS Ni–H		0.0050	1.79×10^{-6}	0.0521
CS Ni-L	0.0050		2.90×10^{-5}	1.58×10^{-4}
CS Ni–He	1.79×10^{-6}	2.90×10^{-5}		2.25×10^{-6}
CS Ni–N_2	0.0521	1.58×10^{-4}	2.25×10^{-6}	

Table 5 – Paired Student's T-test p-values for Peak NER means.

Specimen	CS Ni–H	CS Ni-L	CS Ni–He	CS Ni–N_2
CS Ni–H		2.94×10^{-7}	1.14×10^{-8}	3.88×10^{-6}
CS Ni-L	2.94×10^{-7}		0.191	0.102
CS Ni–He	1.14×10^{-8}	0.191		0.0414
CS Ni–N_2	3.88×10^{-6}	0.102	0.0414	

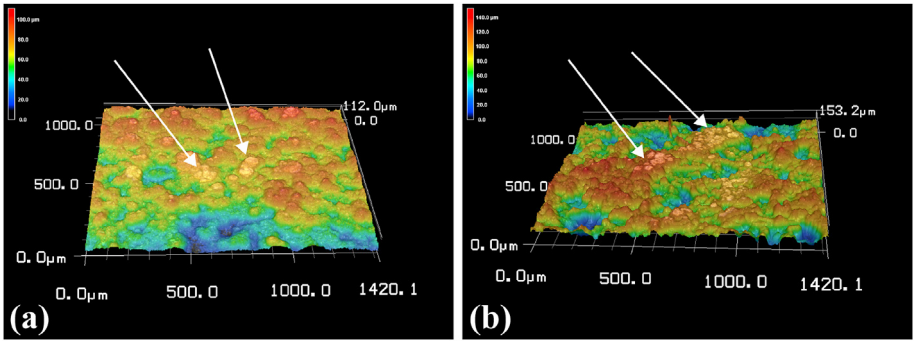

Fig. 8 – Test impressions on specimen surfaces revealed by laser surface profilometry: (a) CS Ni–He, and (b) CS Ni–N_2. The arrows point the slight changes in roughness after QPD test.

resulted in the increased porosity (Fig. 3 and Fig. 4). The increased porosity is due to particles not experiencing enough plastic strain during the deposition process as a result of the greater amount of powder being fed towards the substrate at the same time. This condition leads to a decrease in particle velocity and to a higher interaction between the impinging particles and rebounded particles which may cause deceleration of impinging particles when building at a higher feed rate [31]. The increased porosity contributes to the decreased adhesion strength and greater dissipation of energy in the coating during the QPD testing.

Overall lower energy return was observed, and more successive percussions were required to reach the maximum peak NER values for specimens sprayed in N_2 gas (Fig. 6 and Fig. 7(b)). Powder particles accelerate to lower velocities before impacting the substrate in N_2 compared to that in He. This is attributed to N_2 being a heavier gas than He. This lower impact velocity (i.e. smaller kinetic energy) leads to the powder particles undergoing less plastic deformation upon colliding with the substrate [15,16,32]. Consequently, powder splats sprayed in N_2 are softer and the formed coatings have higher porosity content and a rougher surface. These softer splats on the surface of the sample will therefore strain harden over more percussions. This strain hardening is evident in the initial increase in energy return (i.e. reduction in dissipated energy) from a relatively low value during the first few percussions. The rougher coating surface created when N_2 was used also contributed to the lower initial energy return. The effect of the

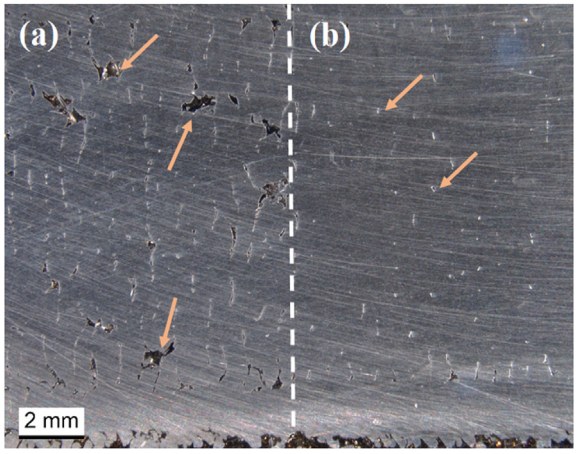

Fig. 9 – Macroscopic image of polished LPDED Ti–6Al–4V showing (a) high porosity near the top and (b) low porosity near the bottom of the specimen. Representative pores are indicated by arrows.

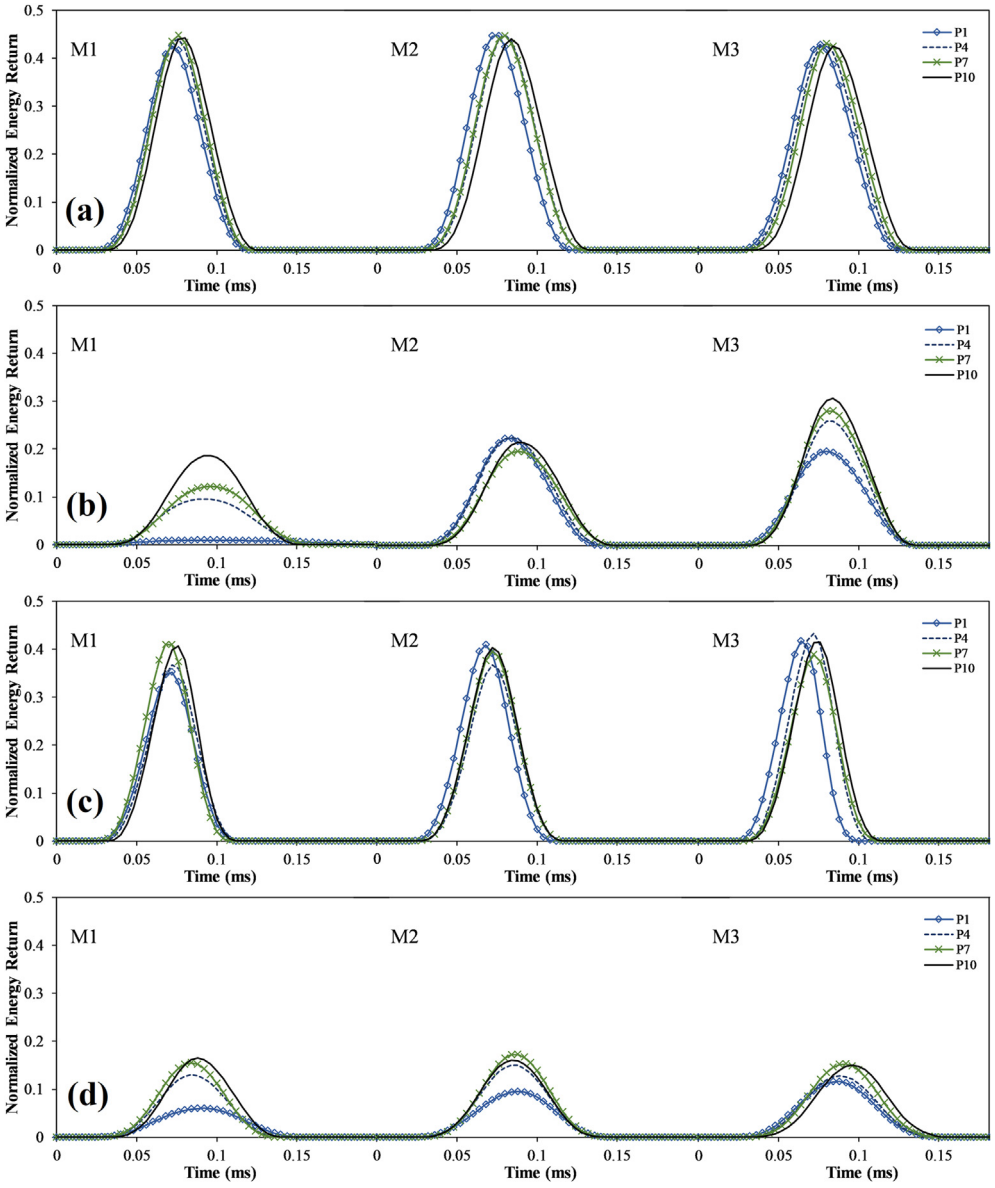

Fig. 10 – NER-time plots for LD Ti64 billet. Plots in (a) are from subsequent tests on the smooth surface near the bottom of the billet (lower internal porosity). Plots in (b) are for the as deposited rough surface near the bottom of the billet (lower internal porosity). Plots in (c) are for the smooth surface near the top of the billet (higher internal porosity), and plots in (d) are for the as deposited rough surface near the top of the billet (higher internal porosity). (M1, M2 and M3 represent three consecutive test measurements at one location on the coating surface, and P1, P4, P7, and P10 represent the first, fourth, seventh, and tenth percussion, respectively).

rough surface on the QPD test data and NER-time plots will be discussed in more detail in section 3.2.

From inspection of Fig. 7 it is noteworthy that for a given specimen the initial and final peak NER values vary from one location to another. This effect can be observed most clearly for the case of the CS Ni–H specimen (Fig. 7(a)) where peak NER results vary considerably between locations. This variation is most likely attributed to differences in local porosity and surface roughness on the specimen surface. Since QPD is sensitive to the properties of the specific location being tested, NER-time plots and peak NER values can change for different locations on a specimen.

Laser microscope profilometry was performed on the tested specimens to characterize the degree of surface damage that might result following QPD testing. Overall, the roughness of the specimen sprayed with N_2 was greater than that for the specimen sprayed with He. In general, residual impressions or surface damage resulting from QPD were very difficult to identify. For rough surfaces (Fig. 8), small changes in surface roughness associated with localized plastic deformation of surface asperities were observed in the QPD test region. However, the observed changes in height of the surface roughness due to QPD were generally less than about 50 μm as shown in Fig. 8. For smooth polished surfaces, no surface deformation or

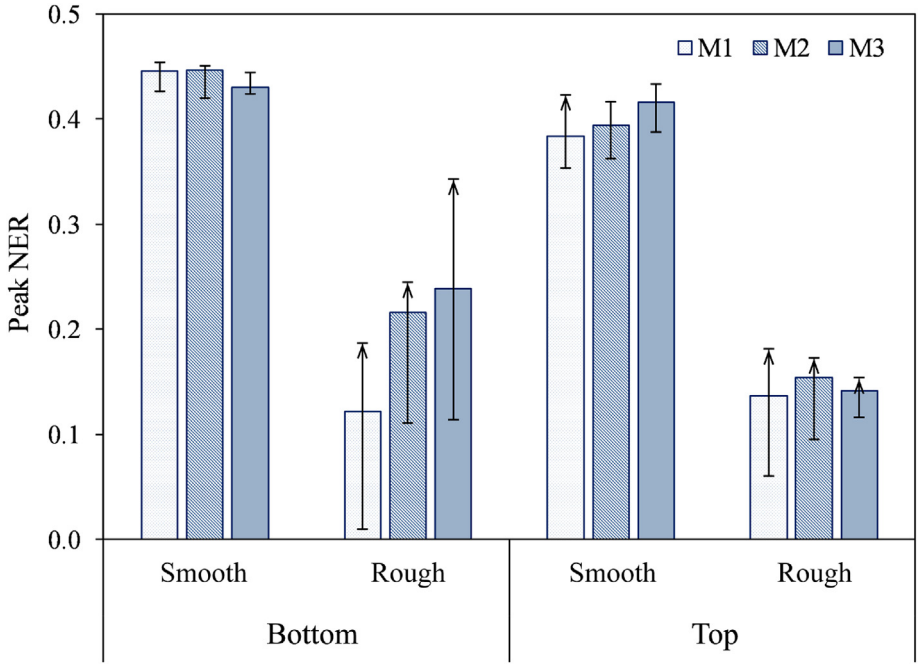

Fig. 11 – Peak NER for the present LD Ti64 billet near the bottom (low internal porosity) and top (high internal porosity) on smooth (polished) and rough (as deposited) surfaces. Each bar shows the median and the start (low value) and end (high value) of the arrows/error bars show the minimum and maximum of peak NER values amongst the 10 percussions.

other indications were observed in the QPD test region. These findings support the notion that QPD is non-destructive when conducted in the manner described in this study.

3.2. *LPDED Ti–6Al–4V*

QPD was used for a laser powder directed energy deposited (LPDED) Ti–6Al–4V billet (Fig. 2) to examine the ability of QPD to detect internal porosity in a specimen created via this additive manufacturing process. Porosity content was varied along the billet, i. e. greater porosity at the top and lower porosity at the bottom, by increasing oxygen gas fed during the deposition. Fig. 9 demonstrates the greater pore number and size at the top of the billet compared to the porosity at the bottom of the billet.

The LD Ti64 specimen was QPD tested on locations at the bottom and top regions with different porosity contents and sizes, and also on both the as deposited (rough) and the polished (smooth) surfaces in order to investigate the effects of the internal porosity and surface condition on test results. Figs. 10 and 11 show NER-time plots and the corresponding peak NER values for the LD Ti64 specimen, respectively. Lower energy return was observed where porosity content was greater regardless of whether a rough or smooth surface was tested. This can be seen by comparing Fig. 10(a) with (c) for smooth surfaces, and Fig. 10(b) with (d) for rough surfaces. Furthermore, the NER was significantly lower for rough surfaces compared to smooth surfaces for the same porosity content (Fig. 10 and Fig. 11). Student's T-test analysis of the smooth surface results for the top paired with those for the bottom of the specimen indicated that these sets were significantly different (p-value $= 1 \times 10^{-10}$), with a mean value of 0.44 at the bottom (low porosity) and 0.39 at the top (high porosity). Since these data were obtained on a smooth surface, they are more indicative of the sensitivity of QPD to internal porosity.

Rough surfaces exhibited energy return data with more variability during the 10 percussions with an overall increasing trend from P1 to P10, and from M1 to M3 (Fig. 10 (b) and (d)). This increase can be attributed to flattening and strain hardening due to plastic deformation of the powders on the surface caused by successive percussions at the same location. The magnitude of this increase eventually reduces as seen by the closer proximity of the NER-time graphs with increasing number of percussions in Fig. 10. By contrast, a relatively small change in the peak energy return with number of percussions was observed for the smooth surface (Figs. 10(a) and (c) and 11). Rougher surfaces undergo greater localized stresses during QPD testing because small surface asperities make contact with the probe resulting in a small contact surface area. Since the probe's initial kinetic energy is constant, these asperity contacts have a significant role in determining how much stress is applied on the contact surface. For the first percussion they are initially relatively soft and under higher stress compared to subsequent percussions. As the asperity regions plastically deform, they become harder while at the same time areas below the asperity contacts come into contact with the probe, increasing the contact area and reducing the average contact stress in the contact region. Consequently, the NER ultimately reaches a maximum value once the average contact stress in the asperity contact regions reaches a critical value, below which localized plastic deformation no longer occurs. We note that a rough surface never becomes fully dense (or

100% contact area) since the NER is always lower than that for the corresponding polished surface. However, the cold spray specimen which ultimately exhibited greater surface roughness also contained greater internal porosity.

4. Conclusions

Efficacy of QPD for evaluating cold sprayed (CS) commercial purity Ni, and for Ti–6Al–4V produced by laser powder directed energy deposition (LPDED) was investigated. The following conclusions were drawn:

1. Increases in porosity were produced in the cold sprayed Ni specimens by increasing the deposition rate with air as the carrier gas, and by altering the carrier gas from He to N_2. An increase in porosity in an LPDED Ti–6Al–4V specimen was also achieved by increasing the oxygen in the process chamber during deposition.
2. Adhesion strength was found to be greater for specimens sprayed with He and N_2 carrier gases compared to that for specimens sprayed with air as the carrier gas. With the exception of Ni sprayed with N_2, adhesion strength was found to be higher with lower amounts of porosity.
3. The higher porosity in CS and LD specimens correlated with lower energy return for QPD as long as adhesion strengths were comparable (i.e. CS Ni–H vs. CS Ni-L and CS Ni–He vs. CS Ni–N_2). Comparisons of QPD data between samples that had relatively large differences in adhesion strength did not necessarily exhibit significant differences in peak energy return despite measurable differences in porosity. This finding appears to be due to other microstructural features, such as increased oxidation and porosity at the substrate interface, that can influence the damping capacity of the specimens.
4. Rough or highly porous surfaces also generally resulted in lower peak energy return than smooth polished surfaces. Rough surfaces also exhibited an increase in the peak energy return with sequential percussions that can be attributed to localized plastic deformation. This increase could reach a maximum within 30 percussions at the same position depending on the specimen surface conditions. Once this maximum was reached, the peak energy return for a rough surface was still lower than that for a smooth surface on the same specimen.
5. While testing smooth surfaces offered a more direct assessment of internal porosity using QPD, greater surface roughness was generally indicated for specimens with more internal porosity.
6. Overall, the present results demonstrated that QPD can provide a rapid assessment of mechanical integrity both in-situ and post processing. As such, QPD has potential for saving much time and labor associated with quality control of additively manufactured parts.

Declaration of Competing Interest

The authors declare the following financial interests/personal relationships which may be considered as potential competing interests: J.C.E. is the co-inventor of quantitative percussion diagnostics (QPD). He co-founded Perimetrics, LLC, as a result of research efforts with this technology and currently maintains a minority stock ownership in the company. Numerous patents have been issued and are pending. The other co-authors have no financial interests or personal relationships that could have appeared to influence the work reported in this paper.

Acknowledgement

The authors would like to thank VRC Metal Systems, LLC (Rapid City, SD) for providing cold spray specimens for this study.

REFERENCES

[1] Sheets CG, Stewart DL, Wu JC, Earthman JC. An in vitro comparison of quantitative percussion diagnostics with a standard technique for determining the presence of cracks in natural teeth. J Prosthet Dent 2014;112:267–75. https://doi.org/10.1016/j.prosdent.2014.02.020.
[2] Dinh A, Sheets CG, Earthman JC. Analysis of percussion response of dental implants: an in vitro study. Mater Sci Eng C 2013;33:2657–63. https://doi.org/10.1016/j.msec.2013.02.033.
[3] Sheets CG, Hui DD, Bajaj V, Earthman JC. Quantitative percussion diagnostics and bone density analysis of the implant-bone interface in a pre- and postmortem human subject. Int J Oral Maxillofac Implants 2013;28:1581–8. https://doi.org/10.11607/jomi.3037.
[4] Poveromo S. Quantitative percussion diagnostics for evaluating bond integrity between composite laminates. Irvine: University of California; 2015.
[5] Poveromo S, Malcolm D, Earthman J. Finite element analysis of quantitative percussion diagnostics for evaluating the strength of bonds between composite laminates. Adv Compos Aerospace, Mar L Appl II 2016:199–212. https://doi.org/10.1007/978-3-319-48141-8_15.
[6] VanSchoiack LR, Wu JC, Sheets CG, Earthman JC. Effect of bone density on the damping behavior of dental implants: an in vitro method. Mater Sci Eng C 2006;26:1307–11. https://doi.org/10.1016/j.msec.2005.08.019.
[7] Stanley BD, Bustemante L, Earthman JC. Novel instrumentation for rapid assessment of internal damage in composite materials. In: Liaw PK, Buck O, Arsenault RJ, REG, editors. Nondestruct. Eval. Mater. Prop. III, the minerals. Metals & Materials Society; 1997. p. 97–100.
[8] Lincoln JD, Rieger LE, Earthman JC. Instrumentation for determining the local damping capacity in honeycomb sandwich composites. J Test Eval 2006;34:232–6. https://doi.org/10.1520/jte12186.
[9] Sheets CG, Wu JC, Rashad S, Phelan M, Earthman JC. In vivo study of the effectiveness of quantitative percussion diagnostics as an indicator of the level of structural pathology of teeth after restoration. J Prosthet Dent 2017;117:218–25. https://doi.org/10.1016/j.prosdent.2016.07.010.
[10] Lu QY, Wong CH. Additive manufacturing process monitoring and control by non-destructive testing techniques: challenges and in-process monitoring. Virtual Phys Prototyp 2018;13:39–48. https://doi.org/10.1080/17452759.2017.1351201.

[11] Klinkov SV, Kosarev VF, Rein M. Cold spray deposition : significance of particle impact phenomena. Aero Sci Technol 2005;9:582–91. https://doi.org/10.1016/j.ast.2005.03.005.
[12] Ajdelsztajn L, Jodoin B, Kim GE, Schoenung JM. Cold spray deposition of nanocrystalline aluminum alloys. Metall Mater Trans 2005;36A:657–66.
[13] Couto M, Dosta S, Guilemany JM. Comparison of the mechanical and electrochemical properties of WC-17 and 12Co coatings onto Al7075-T6 obtained by high velocity oxy-fuel and cold gas spraying. Surf Coating Technol 2015;268:180–9. https://doi.org/10.1016/j.surfcoat.2014.04.034.
[14] Bhattiprolu VS, Johnson KW, Crawford GA. Influence of powder microstructure on the microstructural evolution of as-sprayed and heat treated cold-sprayed Ti-6Al-4V coatings. J Therm Spray Technol 2019;28:174–88. https://doi.org/10.1007/s11666-018-0812-1.
[15] Chavan NM, Ramakrishna M, Phani PS, Rao DS, Sundararajan G. The influence of process parameters and heat treatment on the properties of cold sprayed silver coatings Surface & Coatings Technology the influence of process parameters and heat treatment on the properties of cold sprayed silver coatings. Surf Coating Technol 2011;205:4798–807. https://doi.org/10.1016/j.surfcoat.2011.04.063.
[16] Khun NW, Tan AWY, Bi KJW, Liu E. Effects of working gas on wear and corrosion resistances of cold sprayed Ti-6Al-4V coatings. Surf Coating Technol 2016;302:1–12. https://doi.org/10.1016/j.surfcoat.2016.05.052.
[17] Spencer K, Fabijanic DM, Zhang MX. The use of Al-Al2O3 cold spray coatings to improve the surface properties of magnesium alloys. Surf Coating Technol 2009;204:336–44. https://doi.org/10.1016/j.surfcoat.2009.07.032.
[18] Widener CA, Ozdemir OC, Carter M. Structural repair using cold spray technology for enhanced sustainability of high value assets. Procedia Manuf 2018;21:361–8. https://doi.org/10.1016/j.promfg.2018.02.132.
[19] Garmeh S, Jadidi M, Dolatabadi A. Three-dimensional modeling of cold spray for additive manufacturing. J Therm Spray Technol 2020;29:38–50. https://doi.org/10.1007/s11666-019-00928-3.
[20] Yin S, Cavaliere P, Aldwell B, Jenkins R, Liao H, Li W, et al. Cold spray additive manufacturing and repair: fundamentals and applications. Addit Manuf 2018;21:628–50. https://doi.org/10.1016/j.addma.2018.04.017.
[21] Promoppatum P, Onler R, Yao S. Numerical and experimental investigations of micro and macro characteristics of direct metal laser sintered Ti-6Al-4V products. J Mater Process Technol 2017;240:262–73. https://doi.org/10.1016/j.jmatprotec.2016.10.005.
[22] Lia F, Park JZ, Keist JS, Joshi S, Martukanitz RP. Thermal and microstructural analysis of laser-based directed energy deposition for Ti-6Al-4V and Inconel 625 deposits. Mater Sci Eng, A 2018;717:1–10. https://doi.org/10.1016/j.msea.2018.01.060.
[23] Bobbio LD, Otis RA, Borgonia JP, Dillon RP, Shapiro AA, Liu Z, et al. Additive manufacturing of a functionally graded material from Ti-6Al-4V to invar: experimental characterization and thermodynamic calculations. Acta Mater 2017;127:133–42. https://doi.org/10.1016/j.actamat.2016.12.070.
[24] Hwang T, Woo YY, Han SW, Moon YH. Functionally graded properties in directed-energy-deposition titanium parts. Opt Laser Technol 2018;105:80–8. https://doi.org/10.1016/j.optlastec.2018.02.057.
[25] Liu S, Shin YC. The influences of melting degree of TiC reinforcements on microstructure and mechanical properties of laser direct deposited Ti6Al4V-TiC composites. Mater Des 2017;136:185–95. https://doi.org/10.1016/j.matdes.2017.09.063.
[26] Seo J, Shim D. Effect of track spacing on porosity of metallic foam fabricated by laser melting deposition of Ti6Al4V/TiH2 powder mixture. Vacuum 2018;154:200–7. https://doi.org/10.1016/j.vacuum.2018.04.058.
[27] Sandgren HR, Zhai Y, Lados DA, Shade PA, Schruen JC, Groeber MA, et al. Characterization of fatigue crack growth behavior in LENS fabricated Ti-6Al-4V using high-energy synchrotron x-ray microtomography. Addit Manuf 2016;12:132–41. https://doi.org/10.1016/j.addma.2016.09.002.
[28] ASTM D4541-17. Standard test method for pull-off strength of coatings using portable Adhesion. ASTM Int 2017;1–16. https://doi.org/10.1520/D4541-17.
[29] ASTM E2109-01. Standard test methods for determining area percentage porosity in thermal sprayed coatings. 2014. p. 1–8. https://doi.org/10.1520/E2109-01R14.
[30] Li W-Y, Li C-J, Liao H. Significant influence of particle surface oxidation on deposition efficiency, interface microstructure and adhesive strength of cold-sprayed copper coatings. Appl Surf Sci 2010;256:4953–8. https://doi:10.1016/j.apsusc.2010.03.008.
[31] Lehtonen J, Koivuluoto H, Ge Y, Juselius A, Hannula SP. Cold gas spraying of a high-entropy CrFeNiMn equiatomic alloy. Coatings 2020;10:1–12. https://doi.org/10.3390/coatings10010053.
[32] Bakshi SR, Laha T, Balani K, Agarwal A, Karthikeyan J. Effect of carrier gas on mechanical properties and fracture behaviour of cold sprayed aluminium coatings. Surf Eng 2007;23:18–22. https://doi.org/10.1179/174329407X161618.